

Combination of $t\bar{t}$ cross section measurements and constraints on the mass of the top quark and its decays into charged Higgs bosons

V.M. Abazov³⁷, B. Abbott⁷⁵, M. Abolins⁶⁵, B.S. Acharya³⁰, M. Adams⁵¹, T. Adams⁴⁹, E. Aguilo⁶, M. Ahsan⁵⁹, G.D. Alexeev³⁷, G. Alkhazov⁴¹, A. Alton^{64,a}, G. Alverson⁶³, G.A. Alves², L.S. Ancu³⁶, T. Andeen⁵³, M.S. Anzelc⁵³, M. Aoki⁵⁰, Y. Arnoud¹⁴, M. Arov⁶⁰, M. Arthaud¹⁸, A. Askew^{49,b}, B. Åsman⁴², O. Atramentov^{49,b}, C. Avila⁸, J. BackusMayes⁸², F. Badaud¹³, L. Bagby⁵⁰, B. Baldin⁵⁰, D.V. Bandurin⁵⁹, S. Banerjee³⁰, E. Barberis⁶³, A.-F. Barfuss¹⁵, P. Bargassa⁸⁰, P. Baringer⁵⁸, J. Barreto², J.F. Bartlett⁵⁰, U. Bassler¹⁸, D. Bauer⁴⁴, S. Beale⁶, A. Bean⁵⁸, M. Begalli³, M. Begel⁷³, C. Belanger-Champagne⁴², L. Bellantoni⁵⁰, A. Bellavance⁵⁰, J.A. Benitez⁶⁵, S.B. Beri²⁸, G. Bernardi¹⁷, R. Bernhard²³, I. Bertram⁴³, M. Besançon¹⁸, R. Beuselinck⁴⁴, V.A. Bezzubov⁴⁰, P.C. Bhat⁵⁰, V. Bhatnagar²⁸, G. Blazey⁵², S. Blessing⁴⁹, K. Bloom⁶⁷, A. Boehnlein⁵⁰, D. Boline⁶², T.A. Bolton⁵⁹, E.E. Boos³⁹, G. Borissov⁴³, T. Bose⁶², A. Brandt⁷⁸, R. Brock⁶⁵, G. Brooijmans⁷⁰, A. Bross⁵⁰, D. Brown¹⁹, X.B. Bu⁷, D. Buchholz⁵³, M. Buehler⁸¹, V. Buescher²², V. Bunichev³⁹, S. Burdin^{43,c}, T.H. Burnett⁸², C.P. Buszello⁴⁴, P. Calfayan²⁶, B. Calpas¹⁵, S. Calvet¹⁶, J. Cammin⁷¹, M.A. Carrasco-Lizarraga³⁴, E. Carrera⁴⁹, W. Carvalho³, B.C.K. Casey⁵⁰, H. Castilla-Valdez³⁴, S. Chakrabarti⁷², D. Chakraborty⁵², K.M. Chan⁵⁵, A. Chandra⁴⁸, E. Cheu⁴⁶, S. Chevalier-Théry¹⁸, D.K. Cho⁶², S. Choi³³, B. Choudhary²⁹, T. Christoudias⁴⁴, S. Cihangir⁵⁰, D. Claes⁶⁷, J. Clutter⁵⁸, M. Cooke⁵⁰, W.E. Cooper⁵⁰, M. Corcoran⁸⁰, F. Couderc¹⁸, M.-C. Cousinou¹⁵, S. Crépé-Renaudin¹⁴, V. Cuplov⁵⁹, D. Cutts⁷⁷, M. Ćwiok³¹, A. Das⁴⁶, G. Davies⁴⁴, K. De⁷⁸, S.J. de Jong³⁶, E. De La Cruz-Burelo³⁴, K. DeVaughan⁶⁷, F. Déliot¹⁸, M. Demarteau⁵⁰, R. Demina⁷¹, D. Denisov⁵⁰, S.P. Denisov⁴⁰, S. Desai⁵⁰, H.T. Diehl⁵⁰, M. Diesburg⁵⁰, A. Dominguez⁶⁷, T. Dorland⁸², A. Dubey²⁹, L.V. Dudko³⁹, L. Duflot¹⁶, D. Duggan⁴⁹, A. Duperrin¹⁵, S. Dutt²⁸, A. Dyshkant⁵², M. Eads⁶⁷, D. Edmunds⁶⁵, J. Ellison⁴⁸, V.D. Elvira⁵⁰, Y. Enari⁷⁷, S. Eno⁶¹, P. Ermolov^{39,†}, M. Escalier¹⁵, H. Evans⁵⁴, A. Evdokimov⁷³, V.N. Evdokimov⁴⁰, G. Facini⁶³, A.V. Ferapontov⁵⁹, T. Ferbel^{61,71}, F. Fiedler²⁵, F. Filthaut³⁶, W. Fisher⁵⁰, H.E. Fisk⁵⁰, M. Fortner⁵², H. Fox⁴³, S. Fu⁵⁰, S. Fuess⁵⁰, T. Gadfort⁷⁰, C.F. Galea³⁶, A. Garcia-Bellido⁷¹, V. Gavrilov³⁸, P. Gay¹³, W. Geist¹⁹, W. Geng^{15,65}, C.E. Gerber⁵¹, Y. Gershtein^{49,b}, D. Gillberg⁶, G. Ginther^{50,71}, B. Gómez⁸, A. Goussiou⁸², P.D. Grannis⁷², S. Greder¹⁹, H. Greenlee⁵⁰, Z.D. Greenwood⁶⁰, E.M. Gregores⁴, G. Grenier²⁰, Ph. Gris¹³, J.-F. Grivaz¹⁶, A. Grohsjean²⁶, S. Grünendahl⁵⁰, M.W. Grünewald³¹, F. Guo⁷², J. Guo⁷², G. Gutierrez⁵⁰, P. Gutierrez⁷⁵, A. Haas⁷⁰, N.J. Hadley⁶¹, P. Haefner²⁶, S. Hagopian⁴⁹, J. Haley⁶⁸, I. Hall⁶⁵, R.E. Hall⁴⁷, L. Han⁷, K. Harder⁴⁵, A. Harel⁷¹, J.M. Hauptman⁵⁷, J. Hays⁴⁴, T. Hebbeker²¹, D. Hedin⁵², J.G. Hegeman³⁵, A.P. Heinson⁴⁸, U. Heintz⁶², C. Hensel²⁴, I. Heredia-De La Cruz³⁴, K. Herner⁶⁴, G. Hesketh⁶³, M.D. Hildreth⁵⁵, R. Hirosky⁸¹, T. Hoang⁴⁹, J.D. Hobbs⁷², B. Hoeneisen¹², M. Hohlfeld²², S. Hossain⁷⁵, P. Houben³⁵, Y. Hu⁷², Z. Hubacek¹⁰, N. Huske¹⁷, V. Hynek¹⁰, I. Iashvili⁶⁹, R. Illingworth⁵⁰, A.S. Ito⁵⁰, S. Jabeen⁶², M. Jaffré¹⁶, S. Jain⁷⁵, K. Jakobs²³, D. Jamin¹⁵, C. Jarvis⁶¹, R. Jesik⁴⁴, K. Johns⁴⁶, C. Johnson⁷⁰, M. Johnson⁵⁰, D. Johnston⁶⁷, A. Jonckheere⁵⁰, P. Jonsson⁴⁴, A. Juste⁵⁰, E. Kajfasz¹⁵, D. Karmanov³⁹, P.A. Kasper⁵⁰, I. Katsanos⁶⁷, V. Kaushik⁷⁸, R. Kehoe⁷⁹, S. Kermiche¹⁵, N. Khalatyan⁵⁰, A. Khanov⁷⁶, A. Kharchilava⁶⁹, Y.N. Kharzheev³⁷, D. Khatidze⁷⁰, T.J. Kim³², M.H. Kirby⁵³, M. Kirsch²¹, B. Klima⁵⁰, J.M. Kohl²⁸, J.-P. Konrath²³, A.V. Kozelov⁴⁰, J. Kraus⁶⁵, T. Kuhl²⁵, A. Kumar⁶⁹, A. Kupco¹¹, T. Kurča²⁰, V.A. Kuzmin³⁹, J. Kvita⁹, F. Lacroix¹³, D. Lam⁵⁵, S. Lammers⁵⁴, G. Landsberg⁷⁷, P. Lebrun²⁰, W.M. Lee⁵⁰, A. Leflat³⁹, J. Lellouch¹⁷, J. Li^{78,‡}, L. Li⁴⁸, Q.Z. Li⁵⁰, S.M. Lietti⁵, J.K. Lim³², D. Lincoln⁵⁰, J. Linnemann⁶⁵, V.V. Lipaev⁴⁰, R. Lipton⁵⁰, Y. Liu⁷, Z. Liu⁶, A. Lobodenko⁴¹, M. Lokajicek¹¹, P. Love⁴³, H.J. Lubatti⁸², R. Luna-Garcia^{34,d}, A.L. Lyon⁵⁰, A.K.A. Maciel², D. Mackin⁸⁰, P. Mättig²⁷, A. Magerkurth⁶⁴, P.K. Mal⁸², H.B. Malbouisson³, S. Malik⁶⁷, V.L. Malyshev³⁷, Y. Maravin⁵⁹, B. Martin¹⁴, R. McCarthy⁷², C.L. McGivern⁵⁸, M.M. Meijer³⁶, A. Melnitchouk⁶⁶, L. Mendoza⁸, D. Menezes⁵², P.G. Mercadante⁵, M. Merkin³⁹, K.W. Merritt⁵⁰, A. Meyer²¹, J. Meyer²⁴, J. Mitrevski⁷⁰, R.K. Mommsen⁴⁵, N.K. Mondal³⁰, R.W. Moore⁶, T. Moulik⁵⁸, G.S. Muanza¹⁵, M. Mulhearn⁷⁰, O. Mundal²², L. Mundim³, E. Nagy¹⁵, M. Naimuddin⁵⁰, M. Narain⁷⁷, H.A. Neal⁶⁴, J.P. Negret⁸, P. Neustroev⁴¹, H. Nilsen²³, H. Nogima³, S.F. Novaes⁵, T. Nunnemann²⁶, G. Obrant⁴¹, C. Ochando¹⁶, D. Onoprienko⁵⁹, J. Orduna³⁴, N. Oshima⁵⁰, N. Osman⁴⁴, J. Osta⁵⁵, R. Otec¹⁰, G.J. Otero y Garzón¹, M. Owen⁴⁵, M. Padilla⁴⁸, P. Padley⁸⁰, M. Pangilinan⁷⁷, N. Parashar⁵⁶, S.-J. Park²⁴, S.K. Park³², J. Parsons⁷⁰, R. Partridge⁷⁷, N. Parua⁵⁴, A. Patwa⁷³, G. Pawloski⁸⁰, B. Penning²³, M. Perfilov³⁹, K. Peters⁴⁵, Y. Peters⁴⁵, P. Pétrouff¹⁶, R. Piegai¹, J. Piper⁶⁵, M.-A. Pleier²², P.L.M. Podesta-Lerma^{34,e}, V.M. Podstavkov⁵⁰, Y. Pogorelov⁵⁵, M.-E. Pol², P. Polozov³⁸, A.V. Popov⁴⁰, C. Potter⁶, W.L. Prado da Silva³, S. Protopopescu⁷³, J. Qian⁶⁴, A. Quadt²⁴, B. Quinn⁶⁶, A. Rakitine⁴³, M.S. Rangel¹⁶, K. Ranjan²⁹, P.N. Ratoff⁴³, P. Renkel⁷⁹, P. Rich⁴⁵, M. Rijssenbeek⁷², I. Ripp-Baudot¹⁹,

F. Rizatdinova⁷⁶, S. Robinson⁴⁴, R.F. Rodrigues³, M. Rominsky⁷⁵, C. Royon¹⁸, P. Rubinov⁵⁰, R. Ruchti⁵⁵, G. Safronov³⁸, G. Sajot¹⁴, A. Sánchez-Hernández³⁴, M.P. Sanders¹⁷, B. Sanghi⁵⁰, G. Savage⁵⁰, L. Sawyer⁶⁰, T. Scanlon⁴⁴, D. Schaile²⁶, R.D. Schamberger⁷², Y. Scheglov⁴¹, H. Schellman⁵³, T. Schliephake²⁷, S. Schlobohm⁸², C. Schwanenberger⁴⁵, R. Schwienhorst⁶⁵, J. Sekaric⁴⁹, H. Severini⁷⁵, E. Shabalina²⁴, M. Shamim⁵⁹, V. Shary¹⁸, A.A. Shchukin⁴⁰, R.K. Shivpuri²⁹, V. Siccaldi¹⁹, V. Simak¹⁰, V. Sirotenko⁵⁰, P. Skubic⁷⁵, P. Slattery⁷¹, D. Smirnov⁵⁵, G.R. Snow⁶⁷, J. Snow⁷⁴, S. Snyder⁷³, S. Söldner-Rembold⁴⁵, L. Sonnenschein²¹, A. Sopczak⁴³, M. Sosebee⁷⁸, K. Soustruznik⁹, B. Spurlock⁷⁸, J. Stark¹⁴, V. Stolin³⁸, D.A. Stoyanova⁴⁰, J. Strandberg⁶⁴, S. Strandberg⁴², M.A. Strang⁶⁹, E. Strauss⁷², M. Strauss⁷⁵, R. Ströhmer²⁶, D. Strom⁵³, L. Stutte⁵⁰, S. Sumowidagdo⁴⁹, P. Svoisky³⁶, M. Takahashi⁴⁵, A. Tanasijczuk¹, W. Taylor⁶, B. Tiller²⁶, F. Tissandier¹³, M. Titov¹⁸, V.V. Tokmenin³⁷, I. Torchiani²³, D. Tsybychev⁷², B. Tuchming¹⁸, C. Tully⁶⁸, P.M. Tuts⁷⁰, R. Unalan⁶⁵, L. Uvarov⁴¹, S. Uvarov⁴¹, S. Uzunyan⁵², B. Vachon⁶, P.J. van den Berg³⁵, R. Van Kooten⁵⁴, W.M. van Leeuwen³⁵, N. Varelas⁵¹, E.W. Varnes⁴⁶, I.A. Vasilyev⁴⁰, P. Verdier²⁰, L.S. Vertogradov³⁷, M. Verzocchi⁵⁰, D. Vilanova¹⁸, P. Vint⁴⁴, P. Vokac¹⁰, M. Voutilainen^{67,f}, R. Wagner⁶⁸, H.D. Wahl⁴⁹, M.H.L.S. Wang⁷¹, J. Warchol⁵⁵, G. Watts⁸², M. Wayne⁵⁵, G. Weber²⁵, M. Weber^{50,g}, L. Welty-Rieger⁵⁴, A. Wenger^{23,h}, M. Wetstein⁶¹, A. White⁷⁸, D. Wicke²⁵, M.R.J. Williams⁴³, G.W. Wilson⁵⁸, S.J. Wimpenny⁴⁸, M. Wobisch⁶⁰, D.R. Wood⁶³, T.R. Wyatt⁴⁵, Y. Xie⁷⁷, C. Xu⁶⁴, S. Yacoob⁵³, R. Yamada⁵⁰, W.-C. Yang⁴⁵, T. Yasuda⁵⁰, Y.A. Yatsunenko³⁷, Z. Ye⁵⁰, H. Yin⁷, K. Yip⁷³, H.D. Yoo⁷⁷, S.W. Youn⁵³, J. Yu⁷⁸, C. Zeitnitz²⁷, S. Zelitch⁸¹, T. Zhao⁸², B. Zhou⁶⁴, J. Zhu⁷², M. Zielinski⁷¹, D. Zieminska⁵⁴, L. Zivkovic⁷⁰, V. Zutshi⁵², and E.G. Zverev³⁹

(The DØ Collaboration)

¹Universidad de Buenos Aires, Buenos Aires, Argentina

²LAFEX, Centro Brasileiro de Pesquisas Físicas, Rio de Janeiro, Brazil

³Universidade do Estado do Rio de Janeiro, Rio de Janeiro, Brazil

⁴Universidade Federal do ABC, Santo André, Brazil

⁵Instituto de Física Teórica, Universidade Estadual Paulista, São Paulo, Brazil

⁶University of Alberta, Edmonton, Alberta, Canada; Simon Fraser University, Burnaby, British Columbia, Canada; York University, Toronto, Ontario, Canada and McGill University, Montreal, Quebec, Canada

⁷University of Science and Technology of China, Hefei, People's Republic of China

⁸Universidad de los Andes, Bogotá, Colombia

⁹Center for Particle Physics, Charles University,

Faculty of Mathematics and Physics, Prague, Czech Republic

¹⁰Czech Technical University in Prague, Prague, Czech Republic

¹¹Center for Particle Physics, Institute of Physics, Academy of Sciences of the Czech Republic, Prague, Czech Republic

¹²Universidad San Francisco de Quito, Quito, Ecuador

¹³LPC, Université Blaise Pascal, CNRS/IN2P3, Clermont, France

¹⁴LPSC, Université Joseph Fourier Grenoble 1, CNRS/IN2P3,

Institut National Polytechnique de Grenoble, Grenoble, France

¹⁵CPPM, Aix-Marseille Université, CNRS/IN2P3, Marseille, France

¹⁶LAL, Université Paris-Sud, IN2P3/CNRS, Orsay, France

¹⁷LPNHE, IN2P3/CNRS, Universités Paris VI and VII, Paris, France

¹⁸CEA, Irfu, SPP, Saclay, France

¹⁹IPHC, Université de Strasbourg, CNRS/IN2P3, Strasbourg, France

²⁰IPNL, Université Lyon 1, CNRS/IN2P3, Villeurbanne, France and Université de Lyon, Lyon, France

²¹III. Physikalisches Institut A, RWTH Aachen University, Aachen, Germany

²²Physikalisches Institut, Universität Bonn, Bonn, Germany

²³Physikalisches Institut, Universität Freiburg, Freiburg, Germany

²⁴II. Physikalisches Institut, Georg-August-Universität Göttingen, Germany

²⁵Institut für Physik, Universität Mainz, Mainz, Germany

²⁶Ludwig-Maximilians-Universität München, München, Germany

²⁷Fachbereich Physik, University of Wuppertal, Wuppertal, Germany

²⁸Panjab University, Chandigarh, India

²⁹Delhi University, Delhi, India

³⁰Tata Institute of Fundamental Research, Mumbai, India

³¹University College Dublin, Dublin, Ireland

³²Korea Detector Laboratory, Korea University, Seoul, Korea

³³SungKyunKwan University, Suwon, Korea

³⁴CINVESTAV, Mexico City, Mexico

³⁵FOM-Institute NIKHEF and University of Amsterdam/NIKHEF, Amsterdam, The Netherlands

- ³⁶Radboud University Nijmegen/NIKHEF, Nijmegen, The Netherlands
³⁷Joint Institute for Nuclear Research, Dubna, Russia
³⁸Institute for Theoretical and Experimental Physics, Moscow, Russia
³⁹Moscow State University, Moscow, Russia
⁴⁰Institute for High Energy Physics, Protvino, Russia
⁴¹Petersburg Nuclear Physics Institute, St. Petersburg, Russia
⁴²Stockholm University, Stockholm, Sweden, and Uppsala University, Uppsala, Sweden
⁴³Lancaster University, Lancaster, United Kingdom
⁴⁴Imperial College, London, United Kingdom
⁴⁵University of Manchester, Manchester, United Kingdom
⁴⁶University of Arizona, Tucson, Arizona 85721, USA
⁴⁷California State University, Fresno, California 93740, USA
⁴⁸University of California, Riverside, California 92521, USA
⁴⁹Florida State University, Tallahassee, Florida 32306, USA
⁵⁰Fermi National Accelerator Laboratory, Batavia, Illinois 60510, USA
⁵¹University of Illinois at Chicago, Chicago, Illinois 60607, USA
⁵²Northern Illinois University, DeKalb, Illinois 60115, USA
⁵³Northwestern University, Evanston, Illinois 60208, USA
⁵⁴Indiana University, Bloomington, Indiana 47405, USA
⁵⁵University of Notre Dame, Notre Dame, Indiana 46556, USA
⁵⁶Purdue University Calumet, Hammond, Indiana 46323, USA
⁵⁷Iowa State University, Ames, Iowa 50011, USA
⁵⁸University of Kansas, Lawrence, Kansas 66045, USA
⁵⁹Kansas State University, Manhattan, Kansas 66506, USA
⁶⁰Louisiana Tech University, Ruston, Louisiana 71272, USA
⁶¹University of Maryland, College Park, Maryland 20742, USA
⁶²Boston University, Boston, Massachusetts 02215, USA
⁶³Northeastern University, Boston, Massachusetts 02115, USA
⁶⁴University of Michigan, Ann Arbor, Michigan 48109, USA
⁶⁵Michigan State University, East Lansing, Michigan 48824, USA
⁶⁶University of Mississippi, University, Mississippi 38677, USA
⁶⁷University of Nebraska, Lincoln, Nebraska 68588, USA
⁶⁸Princeton University, Princeton, New Jersey 08544, USA
⁶⁹State University of New York, Buffalo, New York 14260, USA
⁷⁰Columbia University, New York, New York 10027, USA
⁷¹University of Rochester, Rochester, New York 14627, USA
⁷²State University of New York, Stony Brook, New York 11794, USA
⁷³Brookhaven National Laboratory, Upton, New York 11973, USA
⁷⁴Langston University, Langston, Oklahoma 73050, USA
⁷⁵University of Oklahoma, Norman, Oklahoma 73019, USA
⁷⁶Oklahoma State University, Stillwater, Oklahoma 74078, USA
⁷⁷Brown University, Providence, Rhode Island 02912, USA
⁷⁸University of Texas, Arlington, Texas 76019, USA
⁷⁹Southern Methodist University, Dallas, Texas 75275, USA
⁸⁰Rice University, Houston, Texas 77005, USA
⁸¹University of Virginia, Charlottesville, Virginia 22901, USA and
⁸²University of Washington, Seattle, Washington 98195, USA

(Dated: June 3rd 2009)

We combine measurements of the top quark pair production cross section in $p\bar{p}$ collisions in the $\ell+$ jets, $\ell\ell$ and $\tau\ell$ final states (where ℓ is an electron or muon) at a center of mass energy of $\sqrt{s} = 1.96$ TeV in 1 fb^{-1} of data collected with the D0 detector. For a top quark mass of $170 \text{ GeV}/c^2$, we obtain $\sigma_{t\bar{t}} = 8.18_{-0.87}^{+0.98}$ pb in agreement with the theoretical prediction. Based on predictions from higher order quantum chromodynamics, we extract a mass for the top quark from the combined $t\bar{t}$ cross section, consistent with the world average of the top quark mass. In addition, the ratios of $t\bar{t}$ cross sections in different final states are used to set upper limits on the branching fractions $B(t \rightarrow H^+b \rightarrow \tau^+\nu b)$ and $B(t \rightarrow H^+b \rightarrow c\bar{s}b)$ as a function of charged Higgs boson mass.

PACS numbers: 12.15.Ff, 13.85.Lg, 13.85.Qk, 13.85.Rm, 14.65.Ha, 14.80.Cp

Precise measurements of the production and decay properties of the heaviest known fermion, the top quark, provide important tests of the standard model (SM) and

offer a window for searches for new physics. In this paper we measure the top-antitop quark pair ($t\bar{t}$) production cross section and compare it with the SM prediction,

extract the top quark pole mass from this measurement and search for new physics in top quark decays analyzing ratios of the $t\bar{t}$ cross sections measured in different decay channels.

The inclusive $t\bar{t}$ production cross section ($\sigma_{t\bar{t}}$) is measured in different $t\bar{t}$ decay channels assuming SM branching fractions. The comparison of the results to predictions in next-to-leading order perturbative quantum chromodynamics (QCD), including higher order soft gluon resummations [1, 2, 3, 4], yields a direct test of the SM. Ratios of $\sigma_{t\bar{t}}$ measured in different final states are particularly sensitive to non-SM particles that may appear in top quark decays, especially if the boson in the decay is not a SM W boson. An example is the decay into a charged Higgs boson ($t \rightarrow H^+b$), which, as predicted in some models [5], can compete with the SM decay $t \rightarrow W^+b$. Additionally, many experimental uncertainties cancel in the ratios. Furthermore, since $\sigma_{t\bar{t}}$ depends on the mass of the top quark (m_t), it can be used to extract m_t . Such measurement is less accurate than direct mass measurements, but provides complementary information with different experimental and theoretical uncertainties.

Within the SM, each quark of the $t\bar{t}$ pair is expected to decay nearly 100% of the times into a W boson and a b quark [6]. W bosons can decay hadronically into $q\bar{q}'$ pairs or leptonically into $e\nu_e$, $\mu\nu_\mu$ and $\tau\nu_\tau$ with the τ in turn decaying onto an electron, a muon, or hadrons, and associated neutrinos. If one of the W bosons decays hadronically while the other one produces a direct electron or muon or a secondary electron or muon from τ decay, the final state is referred to as the ℓ +jets (or ℓj) channel. If both W bosons decay leptonically, this leads to a dilepton final state containing a pair of electrons, a pair of muons, or an electron and a muon (the $\ell\ell$ channel), or a hadronically decaying tau accompanied either by an electron or a muon (the $\tau\ell$ channel).

Measurements of the individual $t\bar{t}$ cross sections in $\ell\ell$ and $\tau\ell$ channels using about 1 fb^{-1} of $p\bar{p}$ data from the D0 detector at the Fermilab Tevatron collider at $\sqrt{s} = 1.96 \text{ TeV}$ are available in Ref. [7]. In the ℓ +jets channel, we use the same selection and background estimation as in Ref. [8], but a slightly larger dataset and a unified treatment of systematic uncertainties with the $\ell\ell$ and $\tau\ell$ channels. We provide a brief summary of the event selection and analysis procedures below.

In each final state we select data samples enriched in $t\bar{t}$ events by requiring one or two isolated high transverse momentum (p_T) leptons for the ℓ +jets or $\ell\ell$ channel respectively. At least two high p_T jets are required for $\ell\ell$ and $\tau\ell$ events, and at least three for ℓ +jets events. Further, in all but the $e\mu$ channel, large transverse missing energy (\cancel{E}_T) is required to account for the large transverse momenta of neutrinos from W boson or τ lepton decays. In the $e\mu$ final state, a requirement on the sum of the p_T of the highest p_T (leading) lepton and the two leading jets is imposed instead. In the $\mu\mu$ channel, the \cancel{E}_T requirement is supplemented with a requirement on

the significance of the \cancel{E}_T measurement, estimated from the p_T of muons and jets, and their expected resolutions. Additional criteria are applied on the invariant mass of the two opposite charge leptons of the same flavor in the ee and $\mu\mu$ channels to reduce the dominant background from $Z/\gamma^* \rightarrow \ell^+\ell^-$ events. In the ℓ +jets and $\tau\ell$ channels we require a minimum azimuthal angle separation between the \cancel{E}_T vector and the lepton p_T , $\Delta\phi(\ell, \cancel{E}_T)$, to reduce background from multijet events, where jets are misidentified as electron, muon or τ . Details of lepton, jet and \cancel{E}_T identification are provided in Refs. [9, 10]. The final selection in these channels demands at least one identified b jet via a neural-network based algorithm [11]. In the ℓ +jets channel we separate events with one or ≥ 2 b -tagged jets due to their different signal over background ratio and systematic uncertainties.

To simplify the combination and extraction of cross section ratios, all channels are constructed to be mutually exclusive. In particular, events with two identified leptons are excluded from the ℓ +jets selection, and all $\tau\ell$ candidates are removed from the rest of the channels.

The compositions of the samples in the ℓ +jets, $\ell\ell$ and $\tau\ell$ channels are shown in Table I. W +jets production dominates the background for the ℓ +jets events, while multijet production is the most important background in the $\tau\ell$ channel. Background in the $\ell\ell$ channels comes mainly from Z +jets production. In the $\ell\ell$ channel, contributions from W +jets production are part of the multijet background. The smaller contribution from diboson production is included in the category labeled “other background”. This category also includes the contribution from single top quark production in the ℓ +jets and $\tau\ell$ channels. The signal, W +jets and Z +jets backgrounds are simulated using ALPGEN [12] for the matrix element calculation and PYTHIA [13] for parton showering and hadronization. Diboson and single top backgrounds are simulated with the PYTHIA and SINGLETOP [14] generators, respectively. We estimate the multijet background from the control data samples. The difference in the ratio of $t\bar{t}$ and W +jets events in the e +jets and μ +jets final states is the result of the larger efficiency and misidentified lepton rate in the e +jets channel compensating for the lower lepton acceptance ($|\eta| < 1.1$) compared to the μ +jets channel ($|\eta| < 2.0$). In addition, the wider rapidity distribution of the W +jets events compared to $t\bar{t}$ events increases the W +jets background contribution in the μ +jets channel.

To calculate the combined cross section, we define a joint likelihood function as the product of Poisson probabilities for the 14 disjoint subsamples, as listed in Table I. Fourteen additional Poisson terms constrain the multijet background in the ℓ +jets and $\tau\ell$ channels. In particular, for the τe and $\tau\mu$ channels, the multijet background is determined by counting events with an electron or muon and associated τ of the same electric charge, introducing a corresponding Poisson term per channel. In the ℓ +jets channel, we estimate the multijet background separately for each of the eight subchannels by using corresponding

TABLE I: Expected numbers of background and signal events for $\sigma_{t\bar{t}} = 8.18$ pb, observed numbers of data events and measured $\sigma_{t\bar{t}}$ at top mass of 170 GeV/ c^2 . Quoted uncertainties include both statistical and systematic uncertainties, added in quadrature.

Channel	Luminosity(pb $^{-1}$)	W +jets	Z +jets	Multijet	Other bkg	$t\bar{t}$	Total	Observed	$\sigma_{t\bar{t}}$ (pb)
e +jets (3 jets, 1 b tag)	1038	53.4 $^{+6.0}_{-6.0}$	6.0 $^{+1.2}_{-1.2}$	31.5 $^{+3.5}_{-3.5}$	11.4 $^{+1.5}_{-1.4}$	81.7 $^{+6.4}_{-6.7}$	184.0 $^{+9.0}_{-9.2}$	183	8.06 $^{+1.89}_{-1.71}$
μ +jets (3 jets, 1 b tag)	996	59.2 $^{+5.5}_{-5.6}$	6.5 $^{+1.3}_{-1.3}$	9.7 $^{+2.8}_{-2.8}$	9.5 $^{+1.2}_{-1.2}$	59.0 $^{+5.7}_{-5.6}$	143.9 $^{+8.1}_{-8.1}$	133	6.43 $^{+2.22}_{-2.01}$
e +jets (3 jets, ≥ 2 b tags)	1038	5.0 $^{+0.8}_{-0.8}$	0.6 $^{+0.2}_{-0.2}$	2.7 $^{+0.3}_{-0.3}$	2.4 $^{+0.4}_{-0.4}$	30.7 $^{+3.9}_{-3.9}$	41.5 $^{+4.7}_{-4.6}$	40	7.78 $^{+2.41}_{-2.01}$
μ +jets (3 jets, ≥ 2 b tags)	996	5.8 $^{+0.9}_{-0.9}$	0.7 $^{+0.2}_{-0.2}$	1.0 $^{+0.3}_{-0.3}$	2.1 $^{+0.3}_{-0.3}$	23.8 $^{+3.4}_{-3.2}$	33.5 $^{+4.1}_{-3.9}$	31	7.29 $^{+2.73}_{-2.25}$
e +jets (≥ 4 jets, 1 b tag)	1038	8.5 $^{+2.7}_{-2.7}$	2.2 $^{+0.5}_{-0.5}$	7.9 $^{+1.0}_{-1.0}$	3.0 $^{+0.5}_{-0.5}$	81.6 $^{+8.7}_{-9.1}$	103.3 $^{+7.3}_{-7.6}$	113	9.38 $^{+1.82}_{-1.52}$
μ +jets (≥ 4 jets, 1 b tag)	996	13.6 $^{+2.6}_{-2.7}$	2.5 $^{+0.7}_{-0.6}$	0.0 $^{+0.0}_{-0.0}$	2.4 $^{+0.4}_{-0.4}$	65.9 $^{+6.9}_{-7.2}$	84.3 $^{+5.9}_{-6.3}$	99	10.44 $^{+2.11}_{-1.76}$
e +jets (≥ 4 jets, ≥ 2 b tags)	1038	1.0 $^{+0.3}_{-0.3}$	0.2 $^{+0.1}_{-0.1}$	1.1 $^{+0.1}_{-0.1}$	0.9 $^{+0.2}_{-0.2}$	41.7 $^{+6.0}_{-6.0}$	44.9 $^{+6.0}_{-6.0}$	30	5.12 $^{+1.59}_{-1.28}$
μ +jets (≥ 4 jets, ≥ 2 b tags)	996	1.5 $^{+0.4}_{-0.4}$	0.3 $^{+0.1}_{-0.1}$	0.0 $^{+0.0}_{-0.0}$	0.7 $^{+0.1}_{-0.1}$	35.6 $^{+5.0}_{-5.1}$	38.2 $^{+5.1}_{-5.2}$	34	7.60 $^{+2.11}_{-1.70}$
ee	1074		2.3 $^{+0.5}_{-0.5}$	0.6 $^{+0.4}_{-0.4}$	0.5 $^{+0.1}_{-0.1}$	11.6 $^{+1.2}_{-1.2}$	15.0 $^{+1.5}_{-1.5}$	17	9.61 $^{+3.47}_{-2.84}$
$e\mu$ (1 jet)	1070		5.5 $^{+0.7}_{-0.8}$	0.9 $^{+0.3}_{-0.2}$	3.1 $^{+0.7}_{-0.7}$	8.9 $^{+1.4}_{-1.4}$	18.4 $^{+1.9}_{-1.9}$	21	10.61 $^{+5.33}_{-4.23}$
$e\mu$ (≥ 2 jets)	1070		5.4 $^{+0.9}_{-1.0}$	2.6 $^{+0.6}_{-0.5}$	1.4 $^{+0.4}_{-0.4}$	36.4 $^{+3.6}_{-3.6}$	45.8 $^{+4.5}_{-4.5}$	39	6.66 $^{+1.81}_{-1.52}$
$\mu\mu$	1009		5.6 $^{+1.1}_{-1.2}$	0.2 $^{+0.2}_{-0.2}$	0.6 $^{+0.1}_{-0.1}$	9.1 $^{+1.0}_{-1.0}$	15.4 $^{+1.8}_{-1.9}$	12	5.08 $^{+3.82}_{-3.06}$
τe (≥ 1 b tag)	1038	0.6 $^{+0.0}_{-0.1}$	0.6 $^{+0.1}_{-0.1}$	3.0 $^{+1.7}_{-1.7}$	0.2 $^{+0.1}_{-0.1}$	10.7 $^{+1.3}_{-1.3}$	15.0 $^{+2.2}_{-2.2}$	16	8.94 $^{+4.03}_{-3.32}$
$\tau\mu$ (≥ 1 b tag)	996	0.8 $^{+0.1}_{-0.2}$	1.2 $^{+0.3}_{-0.3}$	8.0 $^{+2.8}_{-2.8}$	0.2 $^{+0.0}_{-0.0}$	12.6 $^{+1.4}_{-1.4}$	22.7 $^{+3.2}_{-3.2}$	20	6.40 $^{+3.88}_{-3.43}$

control data samples [15]. Four additional terms arise from applying this same method in evaluating the multi-jet background before b tagging.

Each systematic uncertainty is included in the likelihood function through one free ‘‘nuisance’’ parameter [15]. Each of these parameters is represented by a Gaussian probability density function with zero mean and a standard deviation of one; all are allowed to float in the maximization of the likelihood function, thereby changing the central value of the measured $\sigma_{t\bar{t}}$. Correlations are taken into account by using the same nuisance parameter for a common source of systematic uncertainty in different channels scaled by the corresponding standard deviation each individual channel. Thus, the likelihood function to be maximized is represented by the product

$$\mathcal{L} = \prod_{i=1}^{14} \mathcal{P}(n_i, m_i) \times \prod_{j=1}^{14} \mathcal{P}(n_j, m_j) \times \prod_{k=1}^K \text{SD}_{ik} \times \mathcal{G}(\nu_k; 0, 1), \quad (1)$$

where $\mathcal{P}(n, m)$ is the Poisson probability to observe n events given the expectation of m events. The predicted number of events in each channel is the sum of the predicted background and expected $t\bar{t}$ events, which depends on $\sigma_{t\bar{t}}$. In the product, i runs over the subsamples and j runs over the multijet background subsamples. The Gaussian distributions $\text{SD}_{ik} \times \mathcal{G}(\nu_k; 0, 1)$ describe the systematic uncertainties, K is the total number of independent sources of systematic uncertainty, ν_k are the individual nuisance parameters, and SD_{ik} is one standard deviation for the source of uncertainty k in subsample i .

Systematic uncertainties on the measured $\sigma_{t\bar{t}}$ are evaluated from sources that include electron and muon identification; τ and jet identification and energy calibra-

tion; b -jet identification; modeling of triggers, signal and background; and integrated luminosity. All these uncertainties are treated as fully correlated among channels and between signal and background. Systematic uncertainties arising from limited statistics of data or Monte Carlo samples used in estimating signal or backgrounds are considered to be uncorrelated. A detailed discussion on systematic uncertainties can be found in Refs. [7, 8]. Table II shows a breakdown of uncertainties on the combined cross section. We evaluate the effect from each source by setting all uncertainties to zero except the one in question and redoing the likelihood maximization with respect to only the corresponding nuisance parameter. Since the method allows each uncertainty to change the central value, the total uncertainty on $\sigma_{t\bar{t}}$ differs slightly from the quadratic sum of the statistical and individual systematic uncertainties. The total systematic uncertainty on $\sigma_{t\bar{t}}$ exceeds the statistical contribution. The luminosity uncertainty of 6.1% which enters into the estimation of the majority of the backgrounds and the luminosity measurement of the selected samples is the dominant source of systematic uncertainty.

Table III summarizes the individual $\sigma_{t\bar{t}}$ measurements for the individual channels, as well as some of their combinations. Within uncertainties, all measurements are consistent with each other. The combined cross section for ℓ +jets, $\ell\ell$ and $\tau\ell$ final states for a top quark mass of 170 GeV/ c^2 is evaluated to be

$$\sigma_{t\bar{t}} = 8.18_{-0.87}^{+0.98} \text{ pb}, \quad (2)$$

in agreement with theoretical predictions [1, 2, 3, 4]. The uncertainty is comparable to the one on the cross section combination from different methods in the ℓ +jets channel performed by D0 [8]. The observed number of events

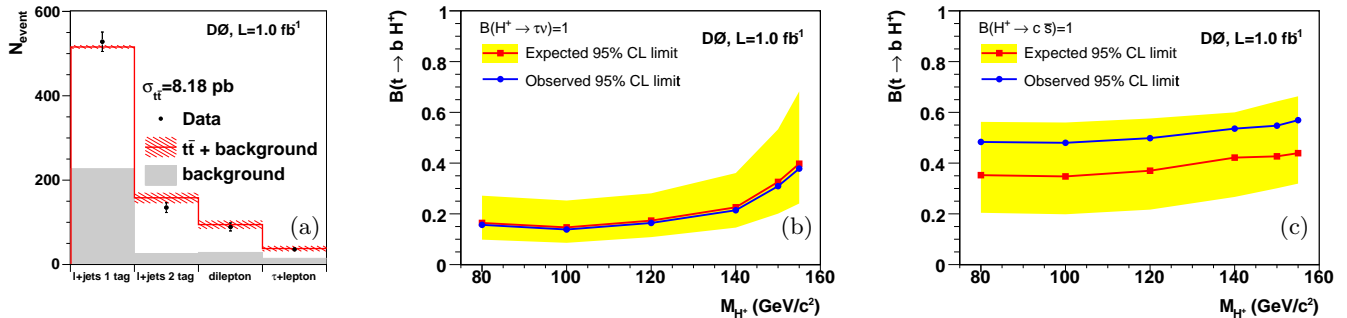


FIG. 1: (a) Expected and observed numbers of events versus channel, used in measuring the combined $\sigma_{t\bar{t}}$. The dashed band around the prediction indicates the total uncertainty. Upper limits on $B(t \rightarrow H^+b)$ for (b) tauonic and (c) leptophobic H^+ decays. The yellow band shows the ± 1 standard deviation band around the expected limit.

TABLE II: Summary of uncertainties on the combined $\sigma_{t\bar{t}}$.

Source	$\Delta\sigma_{t\bar{t}}$ (pb)
Statistical	+0.47 -0.46
Lepton identification	+0.15 -0.14
Tau identification	+0.02 -0.02
Jet identification	+0.11 -0.11
Jet energy scale	+0.19 -0.16
Tau energy scale	+0.02 -0.02
Trigger modeling	+0.11 -0.07
b jet identification	+0.34 -0.32
Signal modeling	+0.17 -0.15
Background estimation	+0.14 -0.14
Multijet background	+0.12 -0.12
Luminosity	+0.56 -0.48
Other	+0.15 -0.14
Total systematic uncertainty	+0.78 -0.69

TABLE III: Summary of measured $\sigma_{t\bar{t}}$ in different channels for $m_t = 170$ GeV/ c^2 .

Channel	$\sigma_{t\bar{t}}$ (pb)
ℓ +jets	$8.46^{+1.09}_{-0.97}$
$\ell\ell$ [7]	$7.46^{+1.60}_{-1.37}$
ℓ +jets and $\ell\ell$	$8.18^{+0.99}_{-0.87}$
$\tau\ell$ [7]	$7.77^{+2.90}_{-2.47}$
ℓ +jets, $\ell\ell$ and $\tau\ell$	$8.18^{+0.98}_{-0.87}$

in the different channels is compared to the sum of the background and combined $t\bar{t}$ signal in Fig. 1(a).

We compute ratios R_σ of measured cross sections, $R_\sigma^{\ell\ell/\ell j} = \sigma_{t\bar{t}}^{\ell\ell}/\sigma_{t\bar{t}}^{\ell j}$ and $R_\sigma^{\tau\ell/\ell\ell-\ell j} = \sigma_{t\bar{t}}^{\tau\ell}/\sigma_{t\bar{t}}^{\ell\ell-\ell j}$, by generating pseudo-datasets in the numerator and denominator in order to take into account the correlation between systematic uncertainties. $\sigma_{t\bar{t}}^{\text{channel}}$ represent the measured cross sections in the corresponding channel. The pseudo-datasets are created by varying the number of signal and background events around the expected number according to Poisson probabilities. All independent sources of

systematic uncertainties are varied within a Gaussian distribution. Although the individual channels considered are exclusive, each channel can receive signal contributions from different $t\bar{t}$ decay modes. We calculate the contribution from dilepton events to the ℓ +jets final state as well as the contribution from dilepton and ℓ +jets events to the $\tau\ell$ final states using the corresponding observed cross sections in the individual channels when generating pseudo-datasets. For each pseudo-dataset, we perform the maximization of Eq. 1 separately in the numerator and denominator, and divide the results. The central value is obtained from the mode of the distribution of R_σ , and the uncertainties are derived from the interval containing 68% of the pseudo-experiments. From these pseudo-experiments we obtain $R_\sigma^{\ell\ell/\ell j} = 0.86^{+0.19}_{-0.17}$ and $R_\sigma^{\tau\ell/\ell\ell-\ell j} = 0.97^{+0.32}_{-0.29}$, which is consistent with the SM expectation of $R_\sigma = 1$.

Extensions of the SM, based on supersymmetry or grand unification [5], require the existence of additional Higgs multiplets beyond the Higgs doublet of the SM. Some of these models, such as the Two Higgs-Doublet Model or the Minimal Supersymmetric Standard Model, foresee the existence of physical degrees of freedom which can be associated with a charged scalar particle, the charged Higgs boson. If this charged Higgs boson is lighter than the top quark, it will appear in the top quark decays. We use the ratios to extract upper limits on the branching ratio $B \equiv B(t \rightarrow H^+b)$. In particular, a charged Higgs boson decaying into a tau and a neutrino ($B(H^+ \rightarrow \tau\nu) = 1$) results in more events in the $\tau\ell$ channel, while fewer events appear in the $\ell\ell$ and ℓ +jets final states compared to the SM prediction. In case of a leptophobic ($B(H^+ \rightarrow c\bar{s}) = 1$) model, the number of dilepton events decreases faster than the number of ℓ +jets events for increasing $B(t \rightarrow H^+b)$. We therefore use $R_\sigma^{\ell\ell/\ell j}$ to set limits on the leptophobic model, while $R_\sigma^{\tau\ell/\ell\ell-\ell j}$ is used to search for decays in which the charged Higgs bosons are assumed to decay exclusively to taus.

To extract the limits, we generate pseudo-datasets assuming different branching fractions $B(t \rightarrow H^+b)$. The signal for a charged Higgs boson is simulated using the PYTHIA Monte Carlo event generator [13], and includes

decays of $t\bar{t} \rightarrow W^+bH^-\bar{b}$ and its charge conjugate (WH) and $t\bar{t} \rightarrow H^+bH^-\bar{b}$ (HH). For a given branching fraction B , we calculate the expected number of $t\bar{t}$ events per final state,

$$N_{t\bar{t}} = [(1-B)^2 \cdot \epsilon_{WW} + 2B(1-B) \cdot \epsilon_{WH} + B^2 \cdot \epsilon_{HH}] \sigma_{t\bar{t}} L, \quad (3)$$

where ϵ are the selection efficiencies for the different decays (WW refers to $t\bar{t} \rightarrow W^+bW^-\bar{b}$) and L is the integrated luminosity. We add $N_{t\bar{t}}$ to the expected background and treat the sum as a new number of expected events in each channel. We then perform the likelihood maximization to extract $\sigma_{t\bar{t}}$ from these pseudo-data as if they contained only SM $t\bar{t}$ production. This provides distributions for the ratios of cross sections for each generated B , which are compared to the observed ratio. We set limits on B by using the frequentist approach of Feldman and Cousins [16].

The observed and expected (i.e., for $R_\sigma = 1$) limits for the tauonic and the leptophobic charged Higgs boson models are shown in Figs. 1(b) and 1(c), respectively. In the tauonic model the upper 95% CL limits on B range from 15% to 40% for $80 \text{ GeV}/c^2 \leq M_{H^\pm} \leq 155 \text{ GeV}/c^2$, improving the limits given in [17]. For the leptophobic charged Higgs boson model, which is investigated here for the first time, the upper limit on B range between 48% and 57% for the same mass range. Although indirect bounds as those from the measured rate of $b \rightarrow s\gamma$ [18] appear stronger than the results from the direct search presented here, they can be invalidated by the presence of new physics contributions.

The interpretation of the direct measurement of the top quark mass [6], has become a subject of intense discussion in terms of its renormalization scheme [19]. The extraction of this parameter from the measured cross section provides complementary information, with different sensitivity to theoretical and experimental uncertainties, relative to direct methods that rely on kinematic details of the top quark reconstruction. Simulated samples of $t\bar{t}$ events generated at different values of the top quark mass are used to estimate the signal acceptance. The resulting measurements of $\sigma_{t\bar{t}}$ are fitted as a function of m_t [2]:

$$\sigma_{t\bar{t}}(m_t) = \frac{1}{m_t^4} [a + b(m_t - m_0) + c(m_t - m_0)^2 + d(m_t - m_0)^3] \quad (4)$$

where $\sigma_{t\bar{t}}$ and m_t are in pb and GeV/c^2 , respectively, and $m_0 = 170 \text{ GeV}/c^2$ [20]. The dependence on the top mass is due to the mass dependence of the selection efficiencies.

We compare this parameterization to a prediction in pure next-to-leading-order (NLO) QCD [1], to a calculation including NLO QCD and all higher-order soft-gluon resummations in next-to-leading logarithms (NLL) [2], to an approximation to the next-to-next-to-leading-order (NNLO) QCD cross section that includes all next-to-next-to-leading logarithms (NNLL) relevant in NNLO QCD [3], and to a calculation that employs full kinematics in the double differential cross section beyond NLL using the soft anomalous dimension matrix to calculate

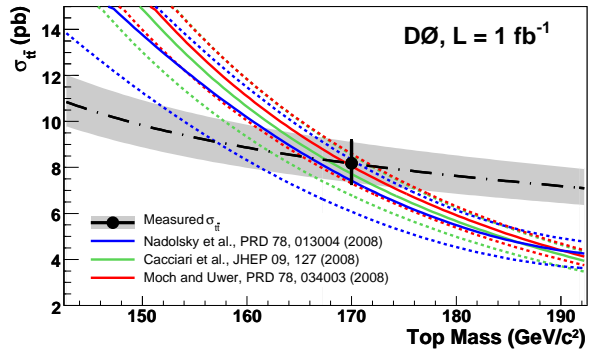


FIG. 2: Experimental and theoretical [1, 2, 3] $\sigma_{t\bar{t}}$ as function of m_t . The colored dashed lines represent the theoretical uncertainties due to the choice of the PDF and the renormalization and factorization scales. The point shows the measured combined $\sigma_{t\bar{t}}$, the black dashed line the fit with Eq. 4 and the gray band the corresponding total experimental uncertainty.

the soft-gluon contributions at NNLO [4]. Figure 2 shows the experimental and the theoretical [1, 2, 3] $t\bar{t}$ cross sections as a function of the top quark mass.

Following the method of Refs. [7, 8], we extract the most probable top quark mass values and the 68% CL band. Since the theoretical predictions are performed in the pole mass scheme, this defines the extracted parameter here. The results are given in Table IV. All values are in good agreement with the current world average of $171.2 \pm 2.1 \text{ GeV}/c^2$ [6].

TABLE IV: Top quark mass with 68% CL region for different theoretical predictions of $\sigma_{t\bar{t}}$. Combined experimental and theoretical uncertainties are shown.

Theoretical prediction	m_t (GeV/c^2)
NLO [1]	$165.5^{+6.1}_{-5.9}$
NLO+NLL [2]	$167.5^{+5.8}_{-5.6}$
approximate NNLO [3]	$169.1^{+5.9}_{-5.2}$
approximate NNLO [4]	$168.2^{+5.9}_{-5.4}$

In summary, we have combined the $t\bar{t}$ cross section measurements in ℓ +jets, $\ell\ell$ and $\tau\ell$ channels to measure $\sigma_{t\bar{t}} = 8.18^{+0.98}_{-0.87}$ pb for a top quark mass of $170 \text{ GeV}/c^2$. For the first time, we have also calculated ratios of cross sections and interpreted them in terms of limits on non-standard model top quark decays into a charged Higgs boson. All results are in good agreement with the SM expectations. Finally, using different theoretical predictions given in the pole mass scheme, we have extracted the top quark mass from the combined $\sigma_{t\bar{t}}$ and have found the result to be consistent with the world average top quark mass [6] from direct measurements.

We thank the staffs at Fermilab and collaborating institutions, and acknowledge support from the DOE and NSF (USA); CEA and CNRS/IN2P3 (France);

FAISI, Rosatom and RFBR (Russia); CNPq, FAPERJ, FAPESP and FUNDUNESP (Brazil); DAE and DST (India); Colciencias (Colombia); CONACyT (Mexico); KRF and KOSEF (Korea); CONICET and UBACyT (Argentina); FOM (The Netherlands); STFC and the Royal Society (United Kingdom); MSMT and GACR (Czech

Republic); CRC Program, CFI, NSERC and WestGrid Project (Canada); BMBF and DFG (Germany); SFI (Ireland); The Swedish Research Council (Sweden); CAS and CNSF (China); and the Alexander von Humboldt Foundation (Germany).

-
- [a] Visitor from Augustana College, Sioux Falls, SD, USA.
 [b] Visitor from Rutgers University, Piscataway, NJ, USA.
 [c] Visitor from The University of Liverpool, Liverpool, UK.
 [d] Visitor from Centro de Investigacion en Computacion - IPN, Mexico City, Mexico.
 [e] Visitor from ECFM, Universidad Autonoma de Sinaloa, Culiacán, Mexico.
 [f] Visitor from Helsinki Institute of Physics, Helsinki, Finland.
 [g] Visitor from Universität Bern, Bern, Switzerland.
 [h] Visitor from Universität Zürich, Zürich, Switzerland.
 [‡] Deceased.
- [1] P. M. Nadolsky *et al.*, Phys. Rev. D **78**, 013004 (2008); W. Beenakker, H. Kuijf, W.L. vanNeerven and J. Smith, Phys. Rev. D **40**, 54 (1989).
 [2] M. Cacciari *et al.*, JHEP **09**, 127 (2008); M. Cacciari, private communications.
 [3] S. Moch and P. Uwer, Phys. Rev. D **78**, 034003 (2008); S. Moch and P. Uwer, private communications.
 [4] N. Kidonakis and R. Vogt, Phys. Rev. D **78**, 074005 (2008); N. Kidonakis, private communications.
 [5] J. Guasch, R. A. Jimenez and J. Sola, Phys. Lett. B **360**, 47 (1995).
 [6] C. Amsler *et al.* [Particle Data Group], Phys. Lett. B **667**, 1 (2008).
 [7] V. M. Abazov *et al.* [D0 Collaboration], Phys. Lett. B **679**, 177 (2009).
 [8] V. M. Abazov *et al.* [D0 Collaboration], Phys. Rev. Lett. **100**, 192004 (2008).
 [9] V. M. Abazov *et al.* [D0 Collaboration], Phys. Rev. D **76**, 092007 (2007).
 [10] V. M. Abazov *et al.* [D0 Collaboration], Phys. Rev. D **76**, 052006 (2007).
 [11] T. Scanlon, Ph.D. thesis, FERMILAB-THESIS-2006-43 (2006).
 [12] M.L. Mangano *et al.*, JHEP **07**, 001 (2003).
 [13] T. Sjöstrand *et al.*, Comput. Phys. Commun. **135**, 238 (2001).
 [14] E.E. Boos *et al.*, Phys. Atom. Nucl. **69**, 1317 (2006).
 [15] V. M. Abazov *et al.* [D0 Collaboration], Phys. Rev. D **74**, 112004 (2006).
 [16] G.J. Feldman and R.D. Cousins, Phys. Rev. D **57**, 3873 (1998).
 [17] A. Abulencia *et al.* [CDF Collaboration], Phys. Rev. Lett. **96**, 042003 (2006).
 [18] M. Misiak *et al.*, Phys. Rev. Lett. **98**, 022002 (2007).
 [19] A. H. Hoang and I. W. Stewart, Nucl. Phys. Proc. Suppl. **185**, 220 (2008).
 [20] We obtain $a = 6.82350 \times 10^9$, $b = 1.10480 \times 10^8$, $c = 8.80552 \times 10^5$ and $d = -1.767 \times 10^3$ for Eq. 4.